

Contrasting behaviour of **suprathermal ⁴He and Fe populations in the interplanetary medium during solar cycle 23 and 24**

BIJOY DALAL,^{1,2} D. CHAKRABARTY,¹ AND N. SRIVASTAVA³

¹*Physical Research Laboratory, Ahmedabad - 380009, India*

²*Indian Institute of Technology Gandhinagar, Gandhinagar - 382055, India*

³*Udaipur Solar Observatory, Physical Research Laboratory, Udaipur - 313001, India*

ABSTRACT

Suprathermal particles (H and other heavy ions like ⁴He, ³He, C, O and Fe) are, in general, characterized by the so-called ‘universal’ -1.5 spectral index. However, variation in this spectral index with composition has not been tested critically. In the present investigation, solar cycle variation of individual ‘quiet’ time suprathermal elements is investigated using $< \sim 1$ MeV/n particle flux data obtained from Ultra Low Energy Isotope Spectrometer on board Advanced Composition Explorer during the solar cycle 23 and 24. The analysis reveals that ⁴He lags the sunspot numbers in solar cycle 24 by almost 700 days and there is no noticeable lag for the 0.07-0.20 MeV/n ⁴He during solar cycle 23. Fe, on the other hand, lags the sunspot variation by almost 300 days in cycle 23 while negligible lag is observed in cycle 24. Further, significant changes in spectral slopes are seen for ⁴He and Fe in the minimum of cycle 24-25 and 23-24 respectively. Although ⁴He and Fe behave differently, all other elements exhibit random lags in both the solar cycles with respect to sunspot numbers and significant changes in spectral slopes are also not observed. These results suggest the contribution of energetic events in the suprathermal ion pool during ‘quiet’ periods. Although no single generation mechanism is found to be adequate to explain these observations, the contrasting behaviour of ⁴He and Fe indicates towards sensitive dependence of the generation of suprathermal population on the first ionization potential and mass to charge ratio.

Keywords: Solar energetic particles(1491) — Corotating streams(314) — Solar wind(1534) — Solar coronal mass ejections(310)

1. INTRODUCTION

Suprathermal particles with energies from ~ 10 KeV per nucleon (keV/n) to ~ 1 MeV per nucleon (MeV/n) are thought to act as seed populations for further acceleration by interplanetary (IP) shocks associated with solar eruptive events like coronal mass ejections (CMEs) (Gosling et al. 1981; Desai et al. 2003, 2004 etc.) and co-rotating interaction regions (CIRs) (e.g., Fisk & Lee 1980; Chottoo et al. 2000; Allen et al. 2019). The two most widely known acceleration mechanisms namely first order Fermi acceleration (or diffusive shock acceleration) (Krymskii 1977; Bell 1978 etc.) and the second order Fermi acceleration (Fermi 1949) necessitate the initial presence of suprathermal particles at the acceleration framework. Energetic protons as well as heavy ions from ⁴He to Fe and beyond constitute suprathermal ion pool in the IP medium. Compositional abundance studies reveal that possible sources of suprathermal ion pool include solar wind ions (Desai et al. 2003), particles associated with previously occurred transient events (Fisk & Lee 1980; Giacalone et al. 2002 etc.), interstellar pick-up ions (Allen et al. 2019) Dominant contribution from the pick-up ions in the suprathermal populations is observed beyond 1 AU (Fisk 1976). Suprathermal particles exhibit power law distribution, also known as ‘quiet’ time tail, when the velocity distribution function (differential directional flux) is plotted against velocity (energy) with a spectral index of -5 (-1.5) (Fisk & Gloeckler 2006, 2007) regardless of the species considered. Henceforth, spectral index in differential flux vs energy convention (-1.5) will be adopted unless otherwise stated. Although suggested to be ‘universal’ in nature, there had been a few reports in the past (e.g. Gloeckler 2003; Mason et al. 2012; Dayeh et al. 2017) that showed that this spectral index deviates substantially from the -1.5 value. It is also not abundantly clear why different elements in the suprathermal ion pool should follow similar

spectral index (Fisk & Gloeckler 2006; Mason et al. 2008). These issues are important and need critical attention as these might throw light on the generation of suprathermal ion population in the IP medium. Enhancements of suprathermal protons and other heavy ions during CIRs within and beyond 1 AU have been reported by many authors (Mason et al. 1997, 2008, 2012; Chotoo et al. 2000; Bučík et al. 2009; Ebert et al. 2012; Filwett et al. 2017; Yu et al. 2018; Allen et al. 2019, 2020 etc.). As a possible source of energization of suprathermal particles associated with CIRs, many have suggested diffusive shock acceleration by the forward and reverse shocks bounding the compression region of CIRs (e.g. Palmer & Gosling 1978; Fisk & Lee 1980). Fisk & Lee (1980) proposed a model in which particles accelerated by shock fronts can be decelerated to lower energies by the effect of adiabatic expansion and associated cooling in the IP medium. However, the spectral rollover predicted by this model below 0.5 MeV/n could not be observed (Mason et al. 1997). The gradual compression region bounded by the shock pair associated with a CIR is also considered as an effective source of acceleration under suitable conditions (Mason 2000; Giacalone et al. 2002), although the shock pairs might not be adequately formed within 1 AU on many occasions. Nevertheless, presence of suprathermal populations in the IP medium in absence of such compression region and shock structures makes it difficult to comprehend the acceleration processes involved. There are evidences that ‘quiet’ time suprathermal particles depend on solar activity. By studying the relative abundances of ‘quiet’ time suprathermal ions at 1 AU, Kecskemety et al. (2011) found out that during minimum of solar cycle, suprathermal Fe/O ratio resembles the corresponding ratio in the solar wind. These results were supported later on by Dayeh et al. (2017), in which solar cycle dependence of suprathermal C/O, Fe/O and $^3\text{He}/^4\text{He}$ with very strong correlations with the averaged sunspot numbers (SSNs) were reported. They argued that suprathermal particles are transported from remote places during the ‘quiet’ times and are accelerated locally. Regardless of the acceleration process involved, it is expected that during the course of transport of the suprathermal particles through the IP medium, the particles may show systematic time delay with solar activity proxies (for example, SSNs) and this may provide important clues for understanding the source of these particle populations. Although indicated in a few earlier works (e.g. Mason et al. 2012; Allen et al. 2019) detailed investigations on these time delays are sparse. Further, comparison of these time delays and spectral indices for various elements for multiple solar cycles may lead to new insights related to the role of solar/IP processes for the generation of these particles. Keeping these issues in mind, the suprathermal particle flux data from the Ultra Low Energy Isotope Spectrometer (ULEIS) (Mason et al. 1998) on board the Advanced Composition Explorer (ACE) (Stone et al. 1998) for solar cycle 23 and 24 have been extensively analyzed and the results are presented in the present work. The results reveal important differences between solar cycle 23 and 24 as far as the above aspects are concerned

2. DATASET

Advanced Composition Explorer or ACE is a spin-stabilized spacecraft revolving around the Lagrangian point (L1) between the Sun and the Earth. In this work, one-hour-integrated differential directional flux data corresponding to different energy channels for H, ^4He , ^3He , O, C and Fe from Mar 01, 1998 to Aug 31, 2020 obtained from the ULEIS on board ACE are used. ULEIS is a time of flight mass spectrometer, which measures the time of flight (τ) and deposited energy (E) of isotopes with $Z=2$ to 28. Using the measured τ and corrected energy (see Mason et al. 1998 for details), mass (M) of the isotope is determined. The dataset spans almost 22 years covering the solar cycles 23 and 24 (henceforth, SC23 and SC24 respectively) and is available at <https://cdaweb.gsfc.nasa.gov/cgi-bin/eval2.cgi>. A list of Co-rotating Interaction Region (CIR) events (Allen et al. 2019) is also used to remove the suprathermal flux enhancements associated with CIR events so that a time series corresponding to ‘quiet’ (discussed in detail in the next section) time can be constructed. Note that the word ‘quiet’ is used here to indicate the absence of any transient suprathermal flux increment event and the applicability of this term will be clear as we progress through this work. The daily averaged sunspot number (SSN) data are available at <http://www.sidc.be/silso/datafiles>.

3. SELECTION OF ‘QUIET’ PERIODS

As indicated in the previous section, the dataset used in the present work pertain to periods devoid of any transient events (e.g. CIR and any other non-CIR events) that cause enhancements in the suprathermal flux. From the entire dataset spanning over 22 years, it is noted that transient CIR or non-CIR events take the flux levels much higher than the background flux level encountered at other times. Therefore, these transient flux variations are apparently easy to remove by choosing a threshold flux level (e.g. Kecskemety et al. 2011). However, in this methodology, the remnant flux for a particular transient event below the threshold level still remains present in the time series. Therefore, we have eliminated the flux variations corresponding to any transient event (short-term fluctuations in the flux data) in

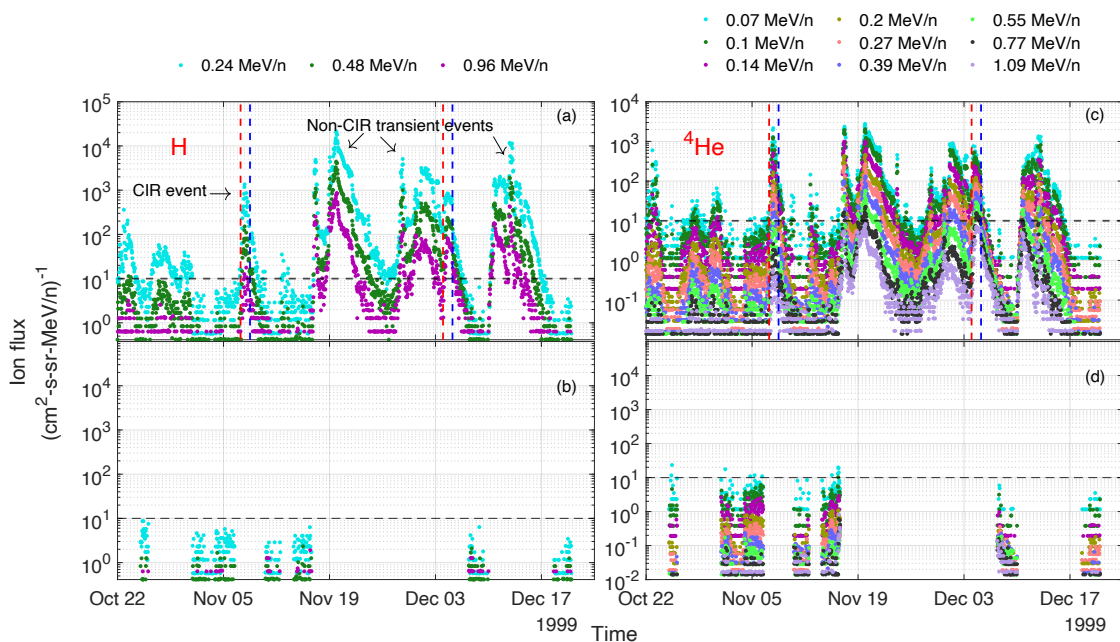


Figure 1. The left column shows the proton flux data (a) before and (b) after the removal of the transient events. The dashed vertical lines indicate the start (red) and end (blue) times of the CIR events during this period as observed by ULEIS/ACE. The non-CIR transient events are indicated by arrows in (a). The black horizontal dashed line is the critical ‘quiet’ time threshold level (10 particles/ (cm²-s-sr-MeV/n)) that emerges after removal of the transient events from the 0.24 MeV/n energy channel for proton. Different energy channels are represented by the mean of the lower and upper energy limits and are shown by colored dots. The right column shows the ⁴He flux variation before (c) and after (d) the removal of transient events similar to what has been done for the proton channel

totality by manually discarding the corresponding fluxes even below the threshold level. This is illustrated in Figure 1. Figure 1(a) and 1(b) show the variations in the proton fluxes for the original and ‘quiet’ dataset (after removal of the transient events in totality) respectively from Oct 22, 1999 to Dec 17, 1999. Different colors correspond to fluxes at different energy channels. The mean of the upper and lower limits of each energy channel is taken to represent the corresponding energy channel and is shown as legend. During the representative interval shown in Figure 1, there were two CIR events, the start and end times of which are marked in red and blue vertical dashed line respectively. The other transient events are termed as ‘non-CIR transient events’ and no attempt is made here to characterize those events. We have verified that all the elements from H to Fe respond to the transient events, although the degree of enhancements vary from one element to the other. Since H is the most abundant element in the suprathermal population, the selection and duration of the transient events have been determined based on the response of ~ 0.24 MeV/n (lowest energy channel available) proton flux. It is observed that a ‘quiet’ time threshold level (shown by a horizontal black dashed line in Figure 1(a) and 1(b)) emerges after the removal of the transient events and this level is close to 10 particles/ (cm²-s-sr-MeV/n) for ~ 0.24 MeV/n H flux. It is checked that this threshold level ensures more than 99.5% of the data points (for 0.24 MeV/n) falling below this level. Once this is ensured, the same time intervals for the transient events are removed from the time series of other elements to obtain the corresponding ‘quiet’ period data. An example is shown in Figure 1(c). It shows the variation of suprathermal ⁴He during the same interval as Figure 1(a) and 1(b). Figure 1(d) is the corresponding ‘quiet’ time ⁴He fluxes obtained after removal of the transient events. There are a total nine energy channels up to ~ 1 MeV/n for ⁴He, that we consider here as the suprathermal energy range.

The complete exclusion of the transient events for the whole duration of the data set is shown in Figure 2. Subplots (a), (c), (e), (g), (i) and, (k) show the temporal variation of suprathermal H, ⁴He, ³He, Fe, C and, O fluxes respectively. Corresponding ‘quiet’ time fluxes are shown in subplot (b), (d), (f), (h) and, (l) respectively. The mean value (up to two decimal place) of each energy channel for H, ⁴He and ³He are mentioned at the left of Figure 2 using colored dots as legends. The same is done for Fe, C and O and mentioned at the right of the figure.

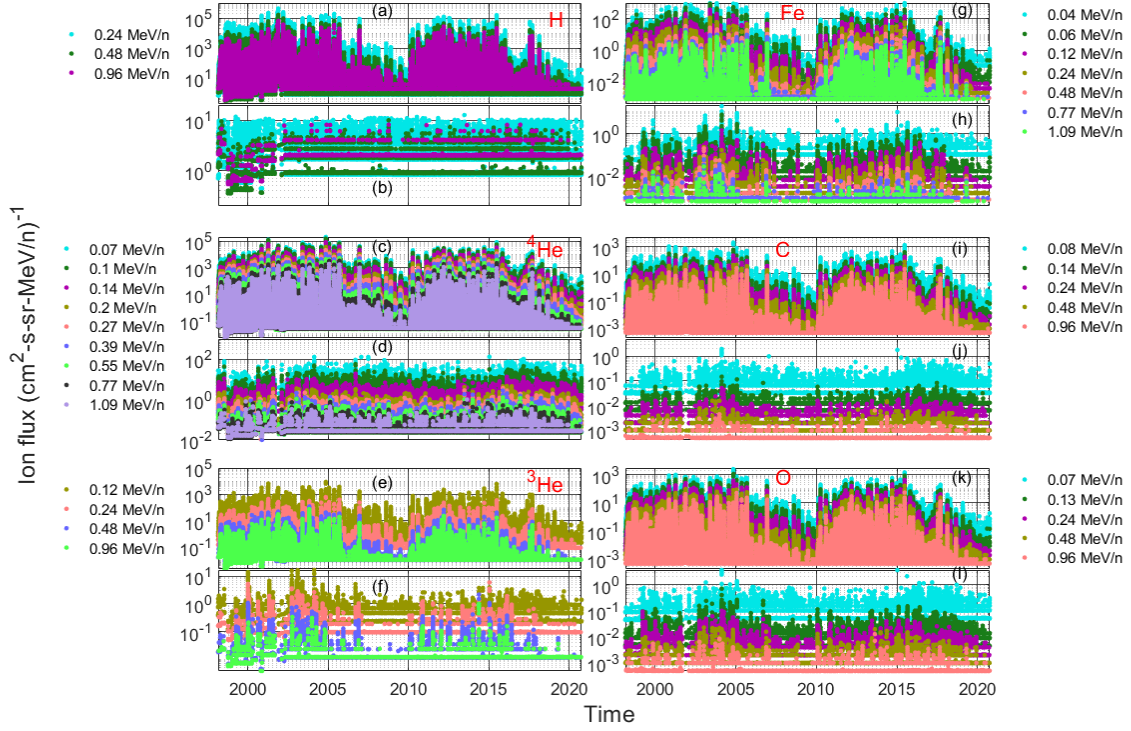


Figure 2. Original vis-à-vis modified (after removal of the transient events) variations of the fluxes of different elements for the entire period. The left column covers the H (original ‘a’ and modified ‘b’), ^4He (original ‘c’ and modified ‘d’) and ^3He (original ‘e’ and modified ‘f’) while the right column is made up with Fe (original ‘g’ and modified ‘h’), C (original ‘i’ and modified ‘j’) and O (original ‘k’ and modified ‘l’). Legends for different energy channels of an element are marked by colored dots and are appropriately placed at the left of right of the plots

Figure 2 reveals that the ‘quiet’ time threshold level of 10 obtained for H can change for other elements when data for two solar cycles are investigated. For example, the threshold level stands around 100 for ^4He . Nevertheless, it can be noted that most of the ‘quiet’ time fluxes lie below the threshold level of 10 if the energy channels < 0.24 MeV/n for ^4He are excluded.

4. RESULTS

4.1. Correlation coefficients and lags with the variations in the sunspot number in SC23 and SC24

Solar cycle variations of the ‘quiet’ time fluxes of various suprathermal elements are shown in Figure 3(a) and Figure 3(b). These figures show the variations in 240 days’ averaged ‘quiet’ time fluxes and SSN for all the elements. Each column corresponds to a particular element (mentioned at the top of each column) and different subplots within a column show the variations in average fluxes for different energies as mentioned in each subplot. The fluxes of ^4He , ^3He , C, O, and Fe are multiplied with 10^2 , 10^3 , 10^4 , 10^3 , and 10^3 respectively for better visual representation. Note that this multiplication has no effect on the calculation of correlation coefficients. Although Figure 3 shows the representative variations in the fluxes and SSN averaged over 240 days, we have also calculated the correlation coefficients and lags for various averaging schemes. In fact, the ‘quiet’ time fluxes and SSN are subjected to averaging over 100 to 400 days in steps of 20 days. In each such step, the lag that yields the maximum Pearson’s correlation coefficient is identified and this step is repeated for every energy channel of each element during SC23 and SC24. The averaging scheme below 100 days is not adopted here as the maximum data gap in all the datasets turns out to be 93 days after removal of the transient events in totality. Subsequently, the means of the maximum cross correlation coefficients (hereafter, CC [F, SSN]) and the corresponding lags (hereafter, L [F, SSN]) along with the standard deviations (calculated based on the outputs obtained for all the steps of data averaging schemes) are tabulated in Table 1. A number of interesting points emerge from this extensive analysis.

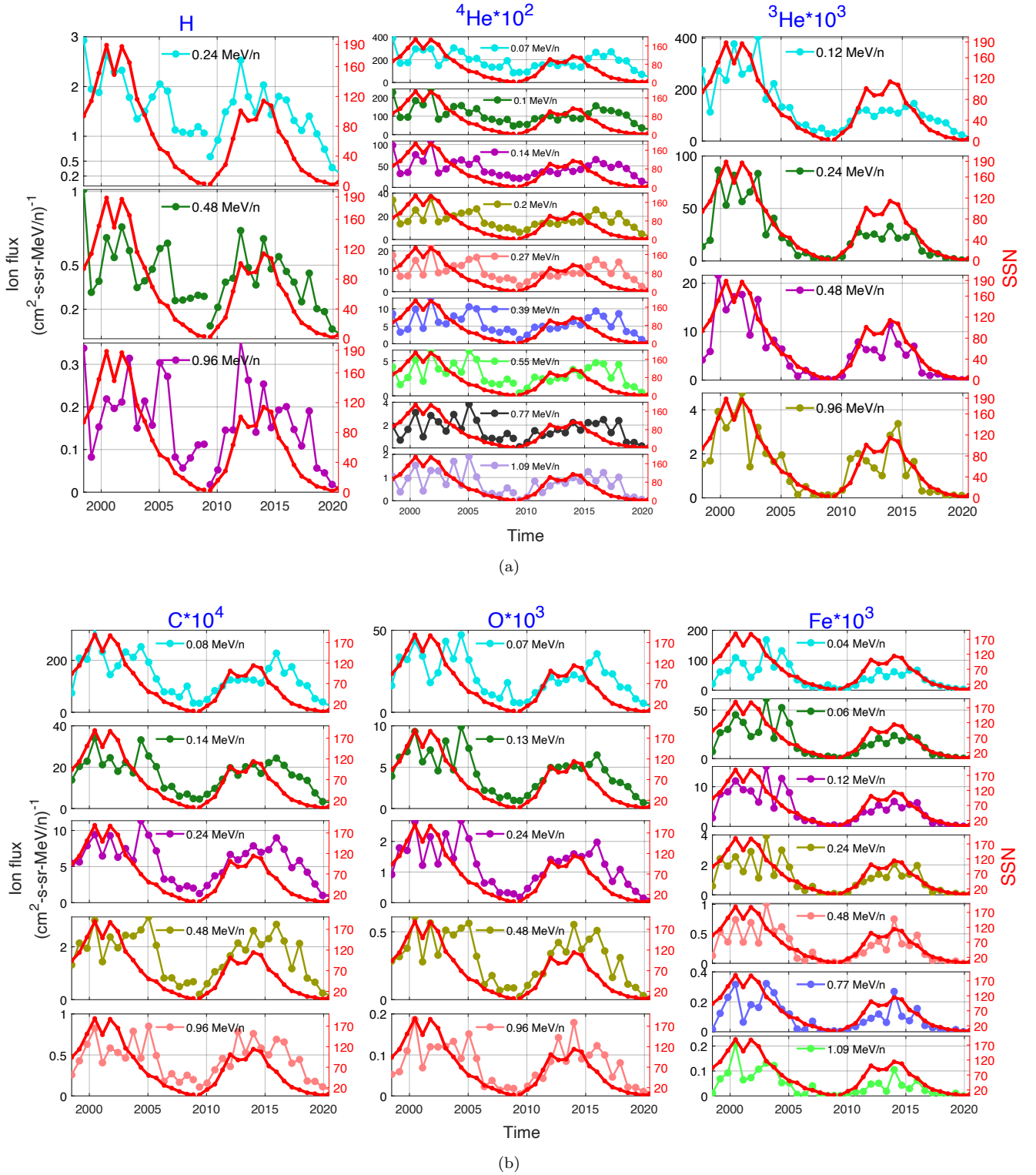


Figure 3. Variations in 240 days' averaged fluxes and SSNs are shown for each suprathermal element and different energy channels. Individual suprathermal elements are mentioned at the top of each panel. Except for H, all other flux values are multiplied by constant factors mentioned at the top of each panel. Different energy channels are marked by different colors

Table 1. Correlation coefficients and lags in SC23 and SC24

Averaging scheme	Element	Energy (MeV/n)	CC [F, SSN]	L [F, SSN] (days)	CC [F, SSN]	L [F, SSN] (days)
100-400 days with a step of 20 days	H	0.24	0.89±0.01	0±0	0.90±0.01	0±0
		0.48	0.86±0.02	0±0	0.92±0.01	0±0
		0.96	0.83±0.03	190±341	0.91±0.02	0±0
	⁴ He	0.07	0.83±0.04	69±149	0.86±0.01	780±81
		0.10	0.84±0.05	49±134	0.86±0.01	699±83
		0.14	0.83±0.04	0±0	0.88±0.01	688±91
		0.20	0.84±0.04	0±0	0.88±0.01	688±91
		0.27	0.83±0.04	396±341	0.88±0.01	715±70
		0.39	0.85±0.03	681±163	0.89±0.02	699±83
		0.55	0.85±0.04	687±170	0.90±0.03	715±70
		0.77	0.85±0.05	699±148	0.88±0.04	664±148
		1.09	0.84±0.05	519±193	0.88±0.05	374±115
	³ He	0.12	0.89±0.05	215±177	0.91±0.01	121±133
		0.24	0.90±0.06	279±94	0.95±0.03	-11±45
		0.48	0.90±0.06	100±155	0.93±0.04	-46±90
	C	0.96	0.92±0.06	59±128	0.89±0.06	-19±52
		0.08	0.92±0.02	312±57	0.90±0.02	583±104
		0.14	0.90±0.03	284±125	0.92±0.01	393±100
		0.24	0.89±0.03	338±108	0.92±0.01	398±125
		0.48	0.89±0.03	359±155	0.93±0.02	374±117
	O	0.96	0.89±0.03	356±98	0.92±0.03	320±55
		0.07	0.89±0.02	356±60	0.92±0.01	538±103
		0.13	0.90±0.03	305±130	0.93±0.01	296±73
		0.24	0.90±0.04	328±101	0.94±0.01	284±102
		0.48	0.91±0.04	391±75	0.95±0.02	313±57
	Fe	0.96	0.91±0.05	338±179	0.93±0.04	308±58
		0.04	0.90±0.04	370±82	0.96±0.02	186±130
		0.06	0.90±0.05	336±71	0.96±0.02	43±92
		0.12	0.90±0.05	326±60	0.95±0.03	30±82
		0.24	0.88±0.07	353±67	0.94±0.03	23±90
	0.48	0.88±0.07	359±66	0.91±0.06	23±90	
	0.77	0.87±0.07	359±66	0.90±0.06	30±93	
	1.09	0.86±0.08	268±150	0.89±0.06	41±100	

NOTE—The means of maximum correlation coefficients denoted by CC [F, SSN] and lags denoted by L [F, SSN] corresponding to different energy channels are shown for SC23 and SC24. F, SSN, CC and L denote flux, sunspot numbers, correlation coefficient and lag respectively. The flux and SSN data are subjected to averaging schemes starting from 100 days to 400 days in steps of 20 days. For a given element and energy channel, the maximum correlation coefficient is obtained at a particular lag. This exercise is repeated for each averaging scheme. The mean CC and L at each energy channel is calculated by taking average of the maximum correlation coefficients obtained for all the averaging schemes. The standard deviations are calculated based on maximum correlation coefficients and lags for all averaging schemes.

It is apparent from Figure 3 and confirmed from Table 1 that CC [F, SSN] corresponding to different energy channels of suprathreshold H are quite high (≥ 0.83) in both SC23 and SC24. It is also noted that CC [F, SSN] increases in SC24. Interestingly, L [F, SSN] for H is nearly zero in both SC23 and SC24 for both 0.24 MeV/n and 0.48 MeV/n

particles. However, for the 0.96 MeV/n particles in SC23, the standard deviation (~ 340 days) is much larger than the calculated mean lag (190 days). Therefore, it is difficult to comment on the lag for the 0.96 MeV/n energy channel. The most striking changes are noticed in ^4He , which is found to behave quite differently in SC23 and SC24. Figure 3 indicates that the averaged ^4He flux and SSN are significantly correlated. Table 1 suggests that the CC [F, SSN] is ≥ 0.83 in both the cycles. However, systematic lags are also noticed at higher energy channels (from 0.27 MeV/n onwards) in SC23 when multiple peaks in the suprathermal ^4He flux come up prominently. It can also be noticed that the lags are conspicuous in SC24 across all the energy channels. These observations get credence from the correlation and lag analyses. In SC23, the L [F, SSN] is small until 0.20 MeV/n and ambiguously high for 0.27 MeV/n wherein standard deviation in the lags (~ 340 days) is equivalent to the mean lag (~ 396 days) itself. However, from 0.39 MeV/n onwards, the lags unambiguously (standard deviation is much less than the lag) increase. Importantly, in SC24, L [F, SSN] seems to be nearly constant (in the range of 663-780 days with less standard deviations) throughout the energy range from ~ 0.07 MeV/n to ~ 0.77 MeV/n with the exception of 1.09 MeV/n when it becomes ~ 373 days. Therefore, L [F, SSN] did not change in SC23 and SC24 as far as the 0.39 MeV/n, 0.55 MeV/n and 0.77 MeV/n energy channels are concerned. The important result that comes out of the present analyses is that the lags are not only consistent but also independent of energy (at least up to 0.77 MeV/n) for suprathermal ^4He in SC24. These behaviors of suprathermal ^4He in SC24 are distinctively different compared to that in SC23 wherein negligible or nearly no lag is observed at least up to 0.20 MeV/n.

As far as the variations in the ^3He fluxes (Figure 3) are concerned, a few points can be noted. The correlation between the variations in ^3He flux and SSN is quite remarkable in both SC23 and SC24. From Table 1, it can be noted that that CC [F, SSN] is mostly above 0.89 across both the solar cycles. However, no consistent pattern in lags is observed in SC23 and SC24. In a few cases, the mean lags turned out to be negative with larger standard deviations. Figure 3 suggests that C and O behave similarly in terms of correlations and lags with SSN in both SC23 and SC24. Table 1 reveals that the CC [F, SSN] for C and O are either close to 0.90 or above in both SC23 and SC24 regardless of the energy channels. Further, there is nearly constant lag (lying within 283-397 days) for all the energies of C and O during both SC23 and SC24 with the exception of the lowest energy channels (0.08 MeV/n for C and 0.07 MeV/n for O) in SC24 when the lag lies between 537-582 days. The standard deviations are also reasonably smaller than the mean lags obtained for all the energy channels of suprathermal C and O.

Fe is the heaviest among the elements that have been investigated in this work. Figure 3 reveals that the variations in the flux of Fe show good correlations with the variations in SSN for all the energy channels. The CC [F, SSN] is 0.86 or more in almost all the cases. It is also noted that as far as the lag is concerned, the lags (267-370 days with reasonably smaller standard deviations) in Fe w.r.t. SSN for all the energy channels show up distinctively in SC23 while in SC24, the lags seem to be negligible. Interestingly, as far as the lags are concerned, the behavior of ^4He (until 0.27 MeV/n in SC23) and Fe (until 0.24 MeV/n in SC23) are mostly opposite in SC23 and SC24.

4.2. Variations in spectral indices of different elements at different phases of SC23 and SC24

In order to evaluate the variabilities of spectral indices of different suprathermal elements during different phases of SC23 and SC24, the SSN data from March 1998 to August 2020 are first sub-grouped into seven equal segments. These are - (1) maximum of SC23 (from 11 November 1999 to 11 November 2001), (2) descending phase of SC23 (from 15 July 2003 to 15 July 2005), (3) minimum of SC23-24 (from 05 July 2007 to 05 July 2009), (4) ascending phase of SC24 (from 24 September 2009 to 24 September 2011), (5) maximum of SC24 (from 20 April 2012 to 20 April 2014), (6) descending phase of SC24 (from 08 July 2015 to 08 July 2017), and (7) minimum of SC24-25 (from 01 October 2018 to 01 October 2020). The duration of each phase is two years. ‘Quiet’ time fluxes of each element are then averaged over each phase and plotted against corresponding energies as shown in Figure 4. Each subplot in Figure 4 corresponds to the spectra of an element mentioned at the right upper corner of each subplot. Every colored dot in the figure is the averaged flux over a phase corresponding to the mean energy of a channel. Lines with seven different colors are the least square fitted lines corresponding to the seven phases of solar cycles as mentioned earlier. The spectral indices denoted by m_i 's (where $i = 1, 2, 3, 4, 5, 6$ and 7) are the estimated slopes of the fitted lines corresponding to different phases. The margin of errors (MoE, which sets a lower and upper bound on the estimated value of a quantity corresponding to some probability) within 95% of confidence bounds in estimating the slopes are also mentioned here. Several important features can be noted from this figure.

Spectral indices for suprathermal H at different phases of solar cycles varies from 1.44 (m_2) to 1.81 (m_4) with a mean of 1.65 except for that at the minimum of SC24-25 25 when it changes to 2.13 (m_7). It can be seen that the spectral

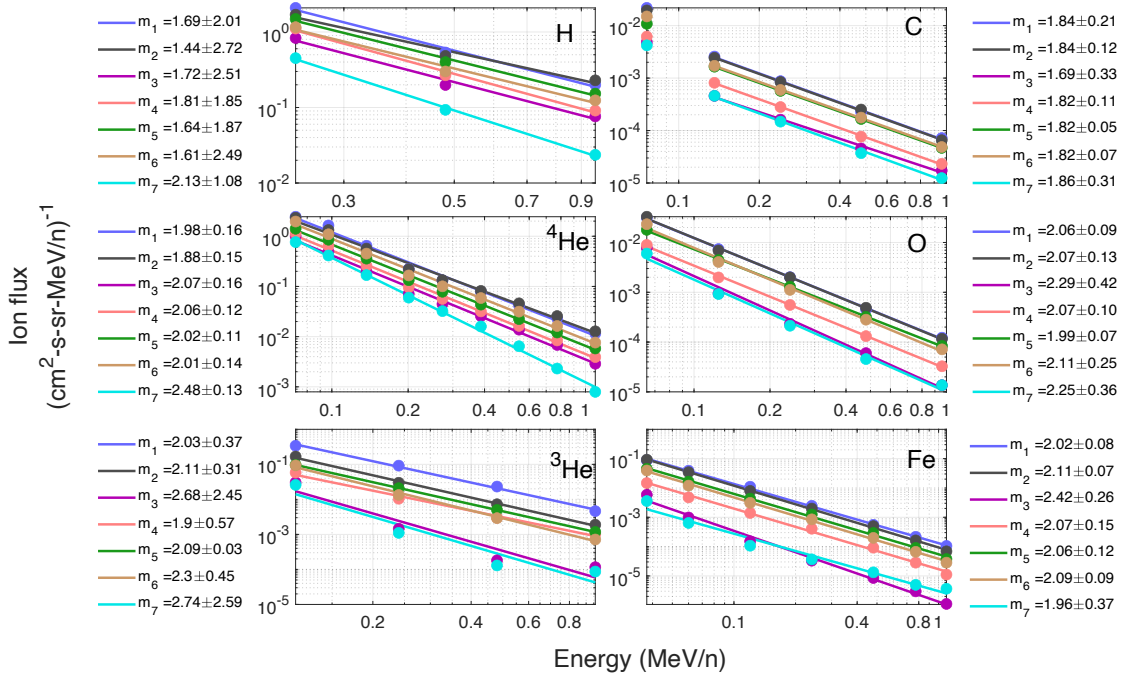


Figure 4. Plots of two years’ ‘quiet’ time averaged differential directional flux vs Energy for the six elements under consideration. Spectral slopes (m_i ’s) of the fitted lines for different phases of solar cycles 23 and 24 are also shown in different colors. C shows power spectra after ~ 0.14 MeV/n. The margin of errors in the spectral index estimation within 95% confidence bounds are written on the left for H, ^4He & ^3He and on the right for C, O & Fe respectively

index changed significantly during the minimum of SC24-25. However, since the number of data points for H is only three (corresponding to three energy channels), the MoE is relatively large. The spectral indices for suprathermal ^4He ranges from 1.88 (m_2) to 2.07 (m_3) till the minimum of SC24-25 when it becomes 2.48 (m_7). Since the number of data points are larger compared to H (9 energy channels compared to 3), the MoE in case of ^4He is significantly lower. Therefore, it is apparent that the spectral index of ^4He shows significant change in the minimum of SC24-25. The spectral indices of ^3He are relatively close to one another (ranges from 1.9 to 2.11) except during the minimum of SC23-24 and the minimum of SC24-25 when these become 2.68 (m_3) and 2.74 (m_7) respectively. In addition, MoE associated with m_3 and m_7 are also low. We have noted that a single linear fitting for C is possible only after 0.14 MeV/n energy channel and the lowest energy channel ($E = 0.08$ MeV/n) does not fit with this line. The reason for this is not clear to us. Interestingly, the spectral indices for all the seven phases are nearly constant for C with a mean value of 1.81 with slight deviation during the minimum of SC23-24 (m_3). The spectral index of O varies from a minimum of 1.99 (m_5) to the maximum of 2.29 (m_3). Therefore, the spectral index during the minimum of SC24-25 is not very different ($m_7=2.25$) from that during the minimum of SC23-24. Interestingly, the spectral index of Fe varies between 1.96 (m_7) and 2.42 (m_3). Further, m_3 turns out to be the maximum spectral index. Unlike ^4He , the spectral index of Fe is substantially greater during the minimum of SC23-24 than the mean index (2.05) at the other six phases. The implications of these results will be discussed in the ensuing section.

5. DISCUSSION

Variations of ‘quiet’-time suprathermal heavy ion ratios (C/O, Fe/O and $^3\text{He}/^4\text{He}$) with solar activity were reported in the past (e.g. Dayeh et al. 2009, 2017; Kecskemety et al. 2011 etc.). It was also suggested that these ratios exhibit SEP-like signature during solar maximum and CIR/solar wind like signature during solar minimum. Therefore, the contribution from SEP and CIR events to the suprathermal ion pool in the IP medium during solar maximum and minimum respectively have been indicated in the past. Our investigation explicitly brings out not only the solar activity dependence but also the time delays between sunspot number (SSN) and ‘quiet’ suprathermal elements. Therefore, our results augment and consolidate the earlier results (e.g. Dayeh et al. 2017) on the solar activity dependence of suprathermal particles in the IP medium. It appears that as the occurrence of SEP (both impulsive and gradual

events) and CIR events vary with the solar activity, so does the suprathermal population in the IP medium. The most striking point in this context emerges when we see conspicuous lags on many occasions despite removal of transient events. This strongly suggests that the so-called ‘quiet’ time suprathermal population in the IP medium is composed of leftover particles from previous solar and IP transient events. Therefore, ‘quiet’ time population of suprathermal population is not ‘quiet’ (even after removal of the transient events) in the true sense of term.

This investigation, for the first time, brings out the distinctive changes in the lags in the ‘quiet’ time suprathermal ^4He in the 0.07 – 0.20 MeV/n energy range in SC24 as compared to SC23. The lags become much higher (~ 700 days) during SC24. Not only that, the spectral index for ‘quiet’ suprathermal ^4He is also shown to change significantly (a change of 0.48 in spectral index) in the minimum of SC24-25 from the mean spectral index (2.00) obtained based on spectral indices of all the other phases. On the contrary, suprathermal Fe (0.04-0.24 MeV/n) shows much lesser lags in SC24 when compared with SC23. Contrasting behavior of Fe is also seen in terms of the variation in spectral index wherein the highest change in the spectral index (2.42) of suprathermal Fe is observed in the minimum of SC23-24 and not in the minimum of SC24-25. Therefore, it is clear that both in terms of lag and spectral index, Fe and ^4He behave in contrasting manners during SC23 and SC24. The possible reasons for these contrasting behaviors are explored in the ensuing paragraphs.

Mason et al. (2012) used the ACE/ULEIS data from 1998 to 2011 and found that CIR event-averaged suprathermal Fe/O lagged behind SSN in SC23 but became more in phase in SC24. The results of Mason et al. (2012) also got extended and supported by the work of Allen et al. (2019) wherein similar behavior for the CIR averaged suprathermal Fe/O (in the energy range of 0.32-0.45 MeV/n) is brought out using ACE/ULEIS data from both SC23 and 24 (1998-2018). Interestingly, the present results that deal with ‘quiet’ time suprathermal populations, show consistency with the results obtained by both Mason et al. (2012) and Allen et al. (2019) as far as the difference in lags of the suprathermal Fe is concerned in both the cycles. If the ‘quiet’ time suprathermal Fe populations have substantial contributions from the previous CIR events, such significant difference in lags are not expected in the two cycles. Keeping in mind that the suprathermal populations that get affected (or may be produced) by (in) the CIR events do remain in the IP medium for a substantially long period, two possibilities can be envisaged to explain this differential behavior in SC23 and SC24. One, the change in the seed population characteristics in both the cycles and/or the change in the acceleration/deceleration mechanisms. At this juncture, it is also important to note that the spectral index of suprathermal Fe also changed in the minimum of SC23-24 rather than in the minimum of SC24-25. Although Dayeh et al. (2017) reported that spectral index of heavy ions may vary from 1.4 to 2.97 in the 0.11 – 0.32 MeV/n range, what the present investigation additionally suggests is the significant change in spectral slope (m_3) of suprathermal Fe during the minimum of SC23-24 in contrast to the minimum of SC24-25. Are the changes in the lag and the spectral slope connected in some way? It is in this context, a discussion on the behavior of suprathermal ^4He is pertinent and more suitable for garnering insight.

The significantly different spectral slope (m_7) of ^4He during the minimum of SC24-25 could well be partly due to the changes in the seed population of suprathermal ^4He in the IP medium. That the CIR associated suprathermal ions could originate from both solar wind and the existing suprathermal ion pool in the heliosphere was suggested by some of the earlier works (e.g. Mason et al. 2008, 2012; Filwett et al. 2017; Allen et al. 2019). However, Mason et al. (2012) and Allen et al. (2019) also suggested that the bulk solar wind does not seem to act directly as seed population for the CIR associated suprathermal abundances for ^4He . In fact, it is suggested that solar wind ^4He ions enter the pre-existing suprathermal ion pool by being energized through unknown processes. It is from this suprathermal ion pool that these ions are further accelerated by CIRs. Therefore, as per this proposition, this is a two-step energization process and it is possible that the flux of ‘quiet’ time suprathermal ^4He at any point of time consists of continually forming suprathermal ^4He ions from solar wind as well as the pre-existing suprathermal ions. Energization of solar wind ^4He during the minimum of SC24-25 might have been adversely impacted so as to cause steeper spectrum with spectral index (m_7) of 2.48. In fact, the recent work of Yogesh et al. (2021) showed that the frequency of occurrence of A_{He} events (A_{He} is the percentage of alpha to proton number density ratio) shifted towards the lower value (A_{He} 2.5 % instead of normal value of 4.5 %) in the solar wind in the speed range 400-500 km/s during SC24. This may suggest less availability of solar wind ^4He for energization and subsequent entry into the pre-existing suprathermal ion pool during the minimum of SC24-25. While the lag is more for ^4He during SC24, the spectral slope of ^4He also changes conspicuously in this cycle. This happens in SC23 for Fe. Although the lags and spectral slopes appear to be connected through various complex physical mechanisms, the consistency in terms of changes in lags and spectral slopes for ^4He and Fe with respect to these two solar cycles is remarkable.

A few other factors also need to be considered here. The acceleration of suprathermal population in the IP medium has also been suggested to depend on M/q (e.g. Drake et al. 2009; Zhao et al. 2017; Reames 2018) and First Ionization Potential (FIP) effects (e.g. Feldman & Widing 2002). Owing to the significant mass and FIP differences, it is possible that the Fe and ^4He behaved in a contrasting manner in SC23 and SC24. More importantly, this also points towards sensitive dependence of the generation of suprathermal population on the FIP and M/q . Although direct evidence in this regard is not available at present, the results from this work provide credence to this proposition. A few other aspects also need attention. Earlier works indirectly support the hypothesis that suprathermal populations in the IP medium might have gone through changes in SC24. Mewaldt et al. (2015) revealed that the fluence of the SEP particles were conspicuously lower during the initial phase of SC24 and this reduction is attributed to two factors – a lower IMF in the IP medium and depletion in the seed population (suprathermal particles). While the reduced IMF reduces the efficiency of acceleration leading to under-population in the SEP energy domain (e.g. Gopalswamy et al. 2014; Mewaldt et al. 2015; Allen et al. 2019), lower densities of seed population may limit the maximum energies that particles can be accelerated to by the Alfvén waves through the wave-particle interaction at the shock front (e.g. Li & Lee 2015). In fact, SC24 is special in many ways. Janardhan et al. (2018) reported unusual polar field and Yogesh et al. (2021) reported significant changes in the solar wind ^4He abundances in this cycle. Another possibility is the changes in the spectral slopes through variations in the pick-up ion populations in the IP medium. It is possible that interstellar pick-up ^4He , energized in distant CIR associated shocks (Fisk & Lee 1980; Gloeckler et al. 1994; Chotoo et al. 2000) and thrown into the inner heliosphere, contributes to the lower energy side of the ^4He flux compensating the deficiencies in ^4He population from the solar wind in SC24 (Yogesh et al. 2021). This can lead to the maintenance of similar flux level at the lower energy side during the minimum of SC24-25. On the other hand, due to lack of reduced solar wind ^4He and weak IMF, the level of ^4He at the higher energy side of suprathermal domain remains low during the minimum of SC24-25 resulting into steeper spectrum of ^4He . Although the changes in IMF, ^4He seed population and pick-up ions, discussed in this section, occur in SC24, we believe that the contrasting behaviour of ^4He and Fe is a potential indicator of the changes in the processes that depend sensitively on the FIP and M/q .

The relative importance of the acceleration and deceleration processes in the changes of suprathermal ^4He that we see during the minimum of SC24-25 also deserves attention at this stage. Dayeh et al. (2017) discussed that suprathermal tails are either generated due to the (1) continuous acceleration of the seed populations in the IP medium (e.g., Fisk & Gloeckler 2006, 2008, 2014; Zank et al. 2014 etc.) or due to the (2) deceleration of energetic particles from the previous solar and IP events (e.g. Fisk & Lee 1980; Giacalone et al. 2002 etc.). Earlier studies have suggested that lower energy part of the CIR (or Stream Interface Region, SIR) associated suprathermal population gets affected primarily by local acceleration processes (e.g., Schwadron et al. 1996; Giacalone et al. 2002; Ebert et al. 2012; Filwett et al. 2017, 2019; Allen et al. 2020, 2021) while the higher energy part gets affected by the shock acceleration occurring far away (e.g., Ebert et al. 2012; Filwett et al. 2019). Therefore, importance of acceleration, whether local or shock induced, is undeniable in the observed changes that are reported in the present investigation. Schwadron et al. (2010) theorized that variable superpositions of stochastic processes (distribution functions represented by exponential and Gaussian functions) could give rise to power law distribution function with exponent of -5 ($f \propto v^{-5}$) (or -1.5 in differential intensity w.r.t. energy approach). This work essentially suggests that variable acceleration and heating processes may be in operation in IP medium for the generation of suprathermal particles. Anteck et al. (2013) adopted stochastic acceleration under pressure balance condition - time scale of acceleration is in balance with timescale of adiabatic cooling in the solar wind as an effective mean of producing -1.5 spectral index. On the other hand, possible role of deceleration processes for the observed changes in the suprathermal ^4He particles during the minimum of SC24-25 cannot be ruled out also. This is because the particles that are accelerated at the distant shock fronts can be thrown back into the inner heliosphere leading to increased scattering and magnetic cooling processes. This may result in modulation in intensity and spectral index (e.g. Fisk & Lee 1980; Mason et al. 1999; Zhao et al. 2016; Allen et al. 2021). Most importantly, particles accelerated through previous transient events, while speeding through the IP medium, experience adiabatic expansion of the solar wind resulting into deceleration of these particles. As a consequence, the energetic particles slow down and enter into the suprathermal pool. According to Fisk & Lee (1980), this type of particles is expected to show a rollover below ~ 0.5 MeV/n in the spectra. However, no such rollover is observed by Mason et al. (1997). We also don't see such rollover feature in the present investigation. Nevertheless, although difficult to comment, the relative role of deceleration processes on the significant changes in the spectral slope of ^4He during SC24-25 cannot be ruled out. It seems therefore reasonable to argue that variable contributions of acceleration and deceleration or distribution functions may lead to variation in spectral indices with the varying

solar activity. These processes might have undergone changes in the minimum of SC23-24 and SC24-25 so as to cause changes in the spectral indices as far as heavier ions like Fe and ^4He are concerned. These aspects need more critical attention in future and the multi-directional suprathermal particle measurements on-board India's forthcoming Aditya-L1 mission (Goyal et al. 2018) may throw important light on some of these issues.

6. CONCLUDING REMARKS

In this work, by analyzing 22 years' of flux variations of suprathermal H, ^4He , ^3He , C, O and Fe from the first Lagrangian point of the Sun-Earth system, we show that these particles follow solar cycle variation with varying lags or time delays. These time delays are shown to vary with energy, element and solar cycle. It is inferred that suprathermal population in the IP medium during 'quiet' times are not free from particles originated from earlier transient events. Further, this investigation, for the first time, reveals that suprathermal Fe and ^4He show most distinctive and contrasting changes in lags and spectral slopes in SC23 and SC24 respectively. It is hypothesized that these changes in lags and spectral slopes may result from either change in production (acceleration/deceleration) process or lack of suitable seed population. Considering the contrasting differences in M/q and FIP of ^4He and Fe, it is suggested that processes that are dependent on M/q and FIP might have played important roles in determining the contrasting behavior of ^4He and Fe in the IP medium during the minimum of SC23 and SC24. Further investigations are needed to understand the underlying physical mechanisms that have determined these contrasting responses of ^4He and Fe.

7. ACKNOWLEDGEMENTS

We are grateful to the Principal Investigator (PI) and all the members of the ULEIS team for constructing the ULEIS instrument and thereafter, generating and managing the dataset used in this work. We also thank WDC-SILSO, Royal Observatory of Belgium, Brussels for the daily estimated sunspot number data used in this paper. This work is supported by the Department of Space, Government of India.

8. DATA SOURCES

The suprathermal particle flux data used in this paper are available at <https://cdaweb.gsfc.nasa.gov/cgi-bin/eval2.cgi>. The daily estimated sunspot number data can be downloaded from <http://www.sidc.be/silso/datafiles>.

REFERENCES

- Allen, R., Mason, G., Ho, G., et al. 2020, *Astronomy & Astrophysics*
- Allen, R., Ho, G., Jian, L., et al. 2021, *Astronomy & Astrophysics*, 650, A25
- Allen, R. C., Ho, G. C., & Mason, G. M. 2019, *The Astrophysical Journal Letters*, 883, L10
- Antecki, T., Schlickeiser, R., & Zhang, M. 2013, *The Astrophysical Journal*, 764, 89
- Bell, A. 1978, *Monthly Notices of the Royal Astronomical Society*, 182, 147
- Bučík, R., Mall, U., Korth, A., & Mason, G. 2009, in *Annales Geophysicae*, Vol. 27, Copernicus GmbH, 3677–3690
- Chotoo, K., Schwadron, N., Mason, G., et al. 2000, *Journal of Geophysical Research: Space Physics*, 105, 23107
- Dayeh, M., Desai, M., Mason, G., Ebert, R., & Farahat, A. 2017, *The Astrophysical Journal*, 835, 155
- Dayeh, M. A., Desai, M. I., Dwyer, J. R., et al. 2009, *The Astrophysical Journal*, 693, 1588, doi: 10.1088/0004-637x/693/2/1588
- Desai, M. I., Mason, G. M., Dwyer, J. R., et al. 2003, *The Astrophysical Journal*, 588, 1149
- Desai, M. I., Mason, G. M., Wiedenbeck, M. E., et al. 2004, *The Astrophysical Journal*, 611, 1156
- Drake, J. F., Cassak, P., Shay, M., Swisdak, M., & Quataert, E. 2009, *The Astrophysical Journal Letters*, 700, L16
- Ebert, R., Dayeh, M., Desai, M., & Mason, G. 2012, *The Astrophysical Journal*, 749, 73
- Feldman, U., & Widing, K. 2002, *Physics of Plasmas*, 9, 629
- Fermi, E. 1949, *Physical review*, 75, 1169
- Filwett, R., Desai, M., Dayeh, M., & Broiles, T. 2017, *The Astrophysical Journal*, 838, 23
- Filwett, R., Desai, M., Ebert, R., & Dayeh, M. 2019, *The Astrophysical Journal*, 876, 88
- Fisk, L., & Gloeckler, G. 2006, *The Astrophysical Journal Letters*, 640, L79
- . 2008, *The Astrophysical Journal*, 686, 1466
- . 2014, *Journal of Geophysical Research: Space Physics*, 119, 8733

- Fisk, L., & Lee, M. 1980, *The Astrophysical Journal*, 237, 620
- Fisk, L. A. 1976, *Journal of Geophysical Research* (1896-1977), 81, 4633, doi: <https://doi.org/10.1029/JA081i025p04633>
- Fisk, L. A., & Gloeckler, G. 2007, *Proceedings of the National Academy of Sciences*, 104, 5749
- Giacalone, J., Jokipii, J. R., & Kota, J. 2002, *The Astrophysical Journal*, 573, 845, doi: [10.1086/340660](https://doi.org/10.1086/340660)
- Gloeckler, G. 2003, in *AIP Conference Proceedings*, Vol. 679, American Institute of Physics, 583–588
- Gloeckler, G., Geiss, J., Roelof, E., et al. 1994, *Journal of Geophysical Research: Space Physics*, 99, 17637
- Gopalswamy, N., Akiyama, S., Yashiro, S., et al. 2014, *Geophysical Research Letters*, 41, 2673
- Gosling, J., Asbridge, J., Bame, S. J., et al. 1981, *Journal of Geophysical Research: Space Physics*, 86, 547
- Goyal, S., Kumar, P., Janardhan, P., et al. 2018, *Planetary and Space Science*, 163, 42
- Janardhan, P., Fujiki, K., Ingale, M., Bisoi, S. K., & Rout, D. 2018, *Astronomy & Astrophysics*, 618, A148
- Kecskemeti, K., Zeldovich, M., & LOGACHEV, Y. 2011, in *Proc. of 32th Int. Cosmic Ray Conference*, Beijing
- Krymskii, G. 1977, in *Akademiia Nauk SSSR Doklady*, Vol. 234, 1306–1308
- Li, G., & Lee, M. A. 2015, *The Astrophysical Journal*, 810, 82
- Mason, G. 2000, in *AIP Conference Proceedings*, Vol. 528, American Institute of Physics, 234–241
- Mason, G., Desai, M., & Li, G. 2012, *The Astrophysical Journal Letters*, 748, L31
- Mason, G., Mazur, J., Dwyer, J., Reames, D., & Von Roseninge, T. 1997, *The Astrophysical Journal Letters*, 486, L149
- Mason, G., Gold, R., Krimigis, S., et al. 1998, *The Advanced Composition Explorer Mission*, 409
- Mason, G., Von Steiger, R., Decker, R., et al. 1999, *Corotating Interaction Regions*, 327
- Mason, G. M., Leske, R. A., Desai, M. I., et al. 2008, *The Astrophysical Journal*, 678, 1458
- Mewaldt, R., Cohen, C., Mason, G., et al. 2015, in *International Cosmic Ray Conference*, Vol. 34, 34th International Cosmic Ray Conference (ICRC2015), 30
- Palmer, I., & Gosling, J. 1978, *Journal of Geophysical Research: Space Physics*, 83, 2037
- Reames, D. V. 2018, *Solar Physics*, 293, 1
- Schwadron, N., Fisk, L., & Gloeckler, G. 1996, *Geophysical research letters*, 23, 2871
- Schwadron, N. A., Dayeh, M., Desai, M., et al. 2010, *The Astrophysical Journal*, 713, 1386
- Stone, E. C., Frandsen, A., Mewaldt, R., et al. 1998, *Space Science Reviews*, 86, 1
- Yogesh, ., Chakrabarty, D., & Srivastava, N. 2021, *Monthly Notices of the Royal Astronomical Society: Letters*, 503, L17, doi: [10.1093/mnrasl/slab016](https://doi.org/10.1093/mnrasl/slab016)
- Yu, J., Berger, L., Drews, C., Wimmer-Schweingruber, R., & Taut, A. 2018, *Astronomy & Astrophysics*, 615, A126
- Zank, G. I., Le Roux, J., Webb, G., Dosch, A., & Khabarova, O. 2014, *The Astrophysical Journal*, 797, 28
- Zhao, L., Zhang, M., & Rassoul, H. K. 2016, *The Astrophysical Journal*, 821, 62
- . 2017, *The Astrophysical Journal*, 836, 31